Wet Stamping of Microscale Periodic Precipitation Patterns

I. T. Bensemann,† M. Fialkowski,† and B. A. Grzybowski*

Department of Chemical Engineering, Northwestern University, 2145 Sheridan Road, Evanston, Illinois 60208

Received: May 17, 2004; In Final Form: August 6, 2004

Although periodic precipitation (PP) phenomena have long attracted scientific interest, their study has been limited to macroscopic systems and simple geometries. An experimental method was developed that allows the generation of highly regular, microscopic PP patterns of arbitrary geometries. Generic scaling laws were established that related the morphologies and topographies of the PP patterns to the geometrical parameters of the system. It was possible to control PP at the level of stochastic phenomena and thus to induce micropatterns of desired chiralities and to control the propagation of defects in them. A 3D nucleation-and-growth model was developed that faithfully reproduced the patterns observed in experiments.

1. Introduction

Since their discovery more than 100 years ago,[1] periodic precipitation (PP) phenomena, that is, phenomena in which the interplay between diffusion and coprecipitation of participating chemicals leads to the emergence of well-defined, periodic bands of precipitation, have attracted considerable scientific interest for their relevance to the issues of nonlinear chemical kinetics,[2−4] wide occurrence in nature,[5−7] and aesthetic appeal.[8] Most of the research on PP has so far focused on macroscopic systems and simple geometries[9−12] (quasi-1D gel columns, single droplets or infinite fronts), for which several empirical laws characterizing the emerging patterns have been formulated.[13,14] At the same time, little is known about PP on the microscale and in complex geometries, mainly because of the lack of suitable experimental techniques that would allow the spatially controlled delivery of participating chemicals. Here, we use the wet stamping (WETS) ref technique to study periodic precipitation induced from arrays of microscopic features of arbitrary shapes stamped onto a surface of a thin film of a dry gel. We show that the periodicity, surface topography, chirality, and propagation of defects in the emerging PP patterns depend on and can be precisely controlled by the dimensions and geometries of the features in the stamp and the thickness of the gel layer. We quantify our observations in the form of generic scaling laws and verify them in 3D simulations based on a probabilistic nucleation-and-growth (NG) model.[15−18]

Typically, PP phenomena are studied in simple geometrical arrangements in which the solution of the so-called outer electrolyte *A* is delivered (as a droplet or semi-infinite front) to the surface of a wet gel containing an inner electrolyte *B*. The diffusion of ions into the wet gel is accompanied by strong backflow/hydrodynamic effects caused by the migration of water to equalize the osmotic pressures. Because the formation of periodic precipitation bands ("rings") requires purely diffusive transport of participating chemicals,[17,18] these hydrodynamic effects suppress the formation of PP patterns in the vicinity of the source of the outer electrolyte. Instead, a uniform transient precipitation zone emerges that usually extends several millimeters from the source,[19] and the first distinct rings observed outside of this zone have macroscopic dimensions (several millimeters in radius and 0.2−10 mm thick; Figure 1a, left).

2. Experimental Section

The technique we developed uses agarose stamps to deliver outer electrolyte into a thin film of dry gelatin uniformly doped with an inner electrolyte. In this system, backflow effects are eliminated, and the transport of ions from agarose into gelatin is a diffusive process.[20,21] Consequently, the dimensions of the transient precipitation zone are minimized, and microscopic PP bands can be resolved. This is illustrated in the right picture in Figure 1a, in which a block of agarose of dimensions similar to those of a droplet shown in the picture on the left was placed onto a dry gel: the first rings appeared $\sim$200 μm from the edge of the stamp, and their dimensions (widths and spacings) were roughly an order of magnitude smaller than those of the rings originating from the drop. All experiments were performed at room temperature.

3. Results and Discussion

Microscale PP in varying geometrical arrangements was studied using stamps patterned in bas relief;[22] in such stamps, each microscopic feature on the stamp's surface acted as a source of periodic precipitation (Figure 1b). In a typical experiment, a stamp was soaked in a solution of silver nitrate (1 M $AgNO_3$) for 2 h and was then placed onto a thin ($H \approx$ 2−120 μm) layer of dry gelatin doped with 0.5% w/w potassium dichromate, $K_2Cr_2O_7$. Once in conformal contact, water from the stamp rapidly wetted the gelatin's surface by capillarity (at the rate of $\sim$1.5 μm/s) and slowly migrated into its bulk (with characteristic diffusion coefficient $D_w \approx 0.5 \times 10^{-6}$ cm^2/s).[23]

When silver cations diffused into the wetted gel, they reacted with dichromate ions to give a brown precipitate, $2AgNO_3 + K_2Cr_2O_7 \rightarrow Ag_2Cr_2O_7\downarrow + 2KNO_3$. The reaction front propagated only when all dichromate anions at a given location had been consumed by the silver cations resupplied diffusively from the stamp; as a result, the reaction front propagated more slowly (with effective diffusion coefficient in the plane of the surface $D_s \approx 10^{-5}$ cm^2/s) than the front of water swelling the gelatin. The reaction−diffusion phenomena took place in a wetted gel layer whose thickness, d_w, could be estimated from $d_w \approx$

* To whom correspondence should be addressed. E-mail: grzybor@northwestern.edu.
† These authors contributed equally to this research.

10.1021/jp047885b CCC: $30.25
Published on Web 11/13/2004

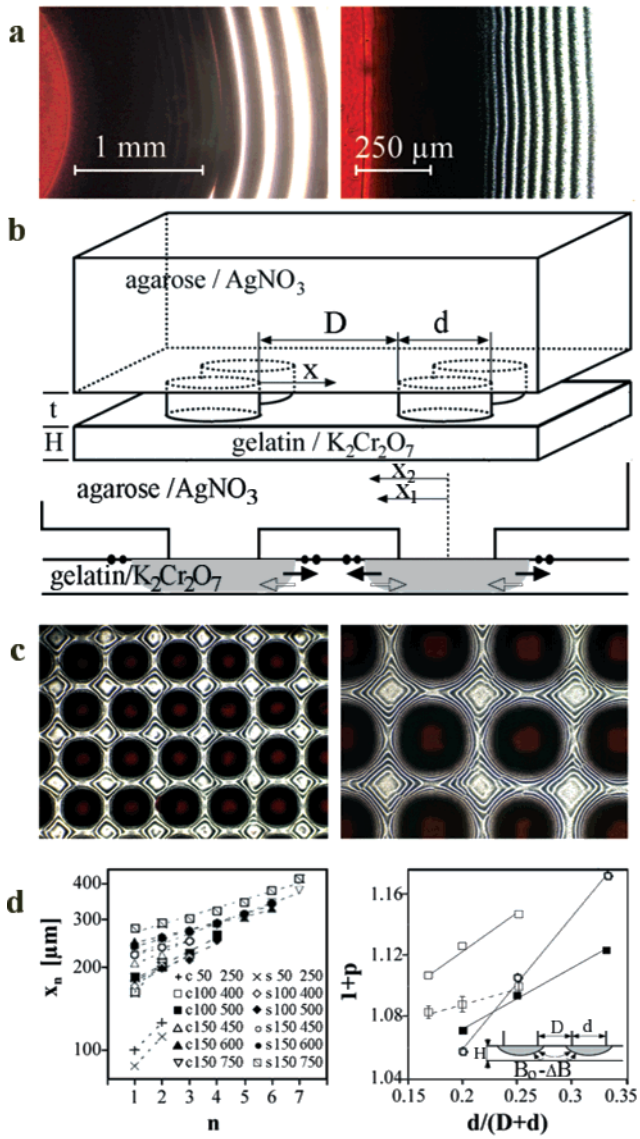

Figure 1. (a) PP patterns obtained from a macroscopic drop of 1M $AgNO_3$ applied onto wet gelatin (left) and from an agarose block of similar dimensions placed on a dry gelatin layer (right); concentrations of inner and outer electrolytes were similar in both cases. (b) Scheme of the experimental arrangement and defined pertinent dimensions: $d = 50-150$ μm, $D = 25-750$ μm, $H = 2-120$ μm, $t = 40$ μm. The gray areas in the lower diagram correspond to transient precipitation zones. The arrows give approximate directions of diffusion of $AgNO_3$ (solid arrows) and $K_2Cr_2O_7$ (open arrows). Positions of PP bands are indicated by solid ovals at the gelatin's surface. (c) Optical micrographs of regular PP patterns obtained by stamping square arrays of circles ($d = 100$ μm, $D = 300$ μm, left picture) and squares ($d = 150$ μm, $D = 600$ μm, right picture). (d) The graph on the left gives the dependence (on a logarithmic vertical scale) of the radius of the nth ring x_n on the ring number in different square arrays of circles or squares. The notation in the legend specifies the shape of the stamped features (c, circles; s, squares), their dimensions (d, (μm), first column) and spacing (D, (μm), second column). All arrays were stamped on 36-μm-thick dry gelatin at least three times. The radii were measured profilometrically. Statistics were collected from three independent stampings for each array and around at least 10 features in each array; in all arrays, the errors were at most on the order of the markers in the graph. The picture on the right shows the dependence of the spacing coefficient, $(1 + p)$, on the feature size-to-period ratio, $d/(D + d)$, for two square arrays of squares ($d = 100$ μm, open squares and $d = 150$ μm, open circles) and for a square array of circles ($d = 150$ μm, full circles). Markers on the dashed line are the results of numerical modeling of three square arrays of squares ($d = 150$ μm, $D = 450$, 600, 750 μm); each point is the average of 10 simulation runs, each starting with a different random seed for r.

$\sqrt{D_w/D_s}L_{char}$, where L_{char} is a characteristic distance the reaction front travels (roughly, half of the spacing between the nearby features in the stamp; hundreds of micrometers). With the measured values of the diffusion coefficients, $d_w \approx 100$ μm, which means that for values of H used in our experiments the gel was wetted all the way to the bottom.

Regular arrays of stamped features gave regular PP patterns (Figure 1c). The morphologies of these patterns depended on the dimensions (d) of and the spacing (D) between the features and on the thickness (H) of the gelatin layer. These dependencies were quantified using stamps with high-symmetry features of, for example, arrays of circles or squares. We found that, as in macroscopic systems, the radii of the rings x_n around each feature obeyed the so-called Jablczynski's law;[13] that is, they increased exponentially with n ($\ln x_n \sim n$; Figure 1d, left). This functional relationship allowed us to quantify the geometry of the rings using the spacing coefficient $1 + p$ defined as $1 + p = x_{n+1}/x_n$. In contrast to macroscopic systems, however, the values of $1 + p$ could be controlled with excellent accuracy by the dimensions of the system.

For a given d, H, and the shape of features, the spacing coefficient was linearly proportional to $d/(d + D)$ (Figure 1d, right). Remarkably, this geometrical dependence could be explained using the Matalon−Packter (MP) law[14] relating $1 + p$ to the initial concentrations of the outer (A_0) and inner (B_0) electrolytes: $(1 + p)(A_0, B_0) = F(B_0) + G(B_0)/A_0$, where $F(B_0)$ and $G(B_0)$ are decreasing functions of B_0. Specifically, prior to the onset of PP, a transient precipitation zone of width proportional to d is rapidly created below each feature. Because all B within this zone is consumed, the inner electrolyte left between the features experiences a sharp concentration gradient and diffuses toward it. Consequently, the effective concentration of B between the features decreases (Figure 1d, right; inset). The amount of this decrease, ΔB, can be estimated from simple geometrical arguments to be $\Delta B/B_0 \approx d/(D + d)$.[24] The spacing coefficient corresponding to the concentration $B_0 - \Delta B$ is then found by expanding the MP law into a power series: $(1 + p)$-$(A_0, B_0 - \Delta B) \approx (1 + p)(A_0, B_0) - \Delta B(F'(B_0) + G'(B_0)/A_0) = \alpha + \beta d/(D + d)$, where for given initial concentrations of electrolytes α and β are positive constants (because the derivatives of F and G functions are both negative).

Changes in the thickness of the gel, H, also had a pronounced effect on the periodicity of the PP patterns. For a constant geometry of the stamped array and for gels thicker than ~15 μm, $1 + p$ increased linearly with increasing H; for thinner gels, the spacing coefficient was a decreasing function of H (Figure 2b). Interestingly, for very thin gels ($H \approx 2$ μm), no periodic precipitation was observed. These effects are vividly illustrated in Figure 2a. The left picture shows a planar PP front traveling from a thinner into a thicker gel: both the absolute spacing between the rings and the value of the $1 + p$ coefficient increase markedly. The picture on the right shows a gel cast onto a polymeric support having wiggly grooves embossed on its surface: the thickness of the gelatin layer in the grooves is ~40 μm, and that on the flat portion of the stamp is ~2 μm. The PP patterns form only in the groves but not on a very thin gel.

The observed trends can be explained by relating H to the effective concentration of the outer electrolyte, A_0^{eff}, in the gel. We have recently shown that very thin ($<\sim$12 μm), ionically doped dry gels show anomalous, markedly decreased absorptivity of ions from solutions of inorganic salts; we have attributed this effect to the existence of a boundary layer near the surface of the support.[25] In the context of the present work, this finding suggests that for small H, A_0^{eff} delivered into gelatin decreases

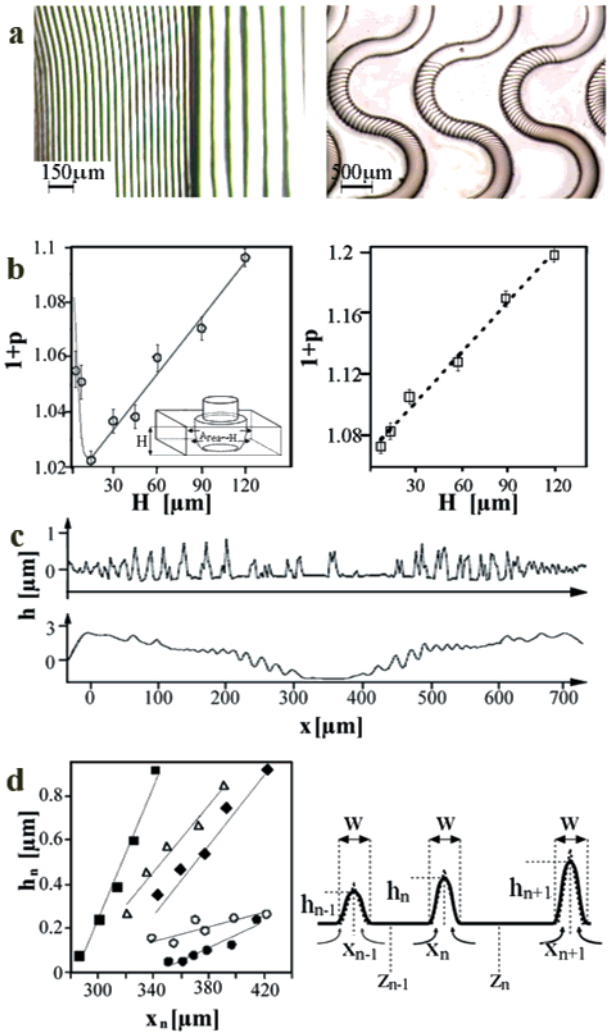

Figure 2. (a) Left picture: both the absolute spacing and the spacing coefficient change when a PP front travels from a thinner ($H = 10$ μm, $1 + p = 1.023$) into a thicker gel ($H = 150$ μm, $1 + p = 1.125$). Right picture: PP from a planar front (from a rectangular block of agarose) does not propagate on very thin (~ 2 μm) portions of the gel and is confined to deeper (~ 40 μm), wiggly grooves. (b) Experimental (left) and simulated (right) dependencies of the spacing coefficient ($1 + p$) on the gel thickness, H, for a square array of circles ($d = 150$ μm, $D = 750$ μm). Errors in the experimental graph are less than 2% of the $1 + p$ values. The inset in the left graph illustrates the origin of the increase of $1 + p$ with H for $H \gtrsim 15$ um. (c) Typical profilograms of PP patterns obtained by applying the same stamp onto a thin (8 μm, upper graph) and a thick (36 μm, lower graph) gelatin layer. Thicker gels swell extensively under the stamped features. (d) Dependence of the height of the nth ridge, h_n, on distance from the center of the feature, x_n, plotted for five gel layer thicknesses: 8 μm (open circles), 25 μm (full circles), 42 μm (full squares), 50 μm (full rhombs), and 65 μm (open triangles). The diagram on the left defines the quantities used to develop pertinent scaling arguments and delineates the boundaries of regions from which silver dichromate is collected into precipitation zones.

with decreasing H. Using the MP law, this decrease translates into an increase in the spacing coefficient. However, when the thickness of the gel is greater than that of the boundary layer, silver cations delivered from the stamp[26] diffuse and react in a wetted layer whose thickness is proportional to H (because $d_w \geq H$ in our experiments). Therefore, the cross-sectional area of the flow of cations traveling in the plane of the gel surface is proportional to H (Figure 2b, left; inset), and their effective input concentration decreases with increasing thickness of the gelatin layer, $A_0^{\text{eff}} \sim A_0/H$. Thus, for fixed geometrical parameters of the array, the MP law predicts $(1 + p)(H) \approx \alpha' + \beta' H$, with α' and β' being some constants.

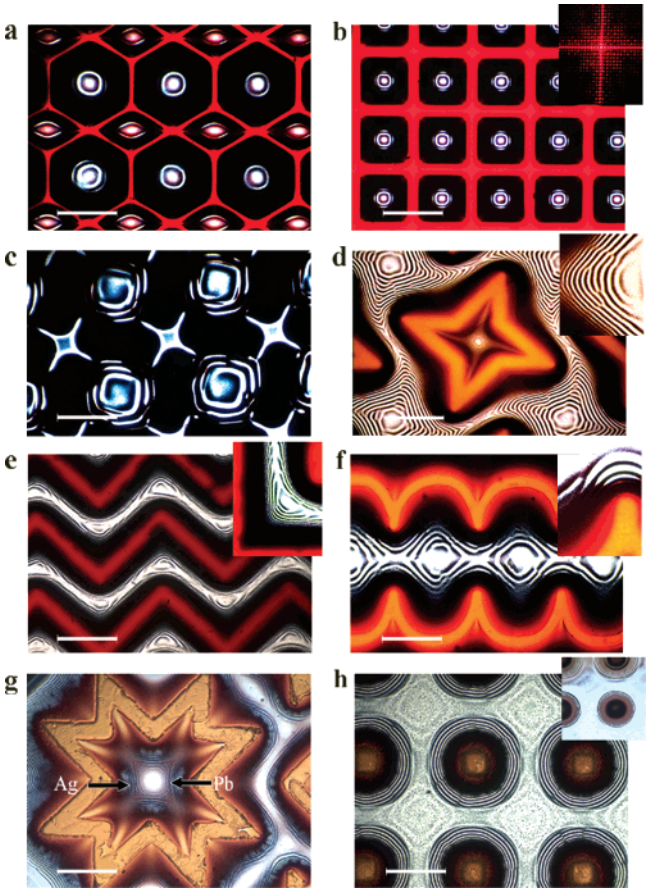

Figure 3. (a and b) PP patterns obtained by stamping connected (network) arrays of features corresponding to the red portions of the images. The highly regular array in b was used as a diffraction grating that upon irradiation with a 632-nm laser produced a diffraction pattern shown in the inset. (c) Spiral originating from a stamped pattern of the same chirality. (d) Wedge dislocations propagating along the diagonals of squares between the arms of the stamped stars. (e) Band multiplications develop at the sharp turns in zigzag geometries. Loop-in-band defects around the tips of stamped "spikes" are shown in f. The insets in d−f are close-ups of the dislocations around individual features. Pictures in g and h show multicomponent PP patterns obtained in a system in which the stamp was soaked in a 3:1 (mol/mol) solution of silver nitrate and lead nitrate. The Liesegang structures that developed had two types of rings differing both in composition and in periodicity. The rings close to the stamped features were made of lead dichromate, whereas those farther from the feature were made of silver dichromate. The composition of the rings was confirmed by two chemical tests: when the fully developed pattern was flooded with KOH (selectively dissolving $PbCr_2O_7$), the inner rings disappeared; when it was flooded with ammonia (dissolving $Ag_2Cr_2O_7$), the outer rings vanished. The inset in h shows the surface after flooding with ammonia. (a−g) All patterns were stamped on 36-μm-thick dry gelatin doped with 0.5% w/w $K_2Cr_2O_7$; the scale bars correspond to 500 μm.

Microscopic PP leads to the formation of regular arrays of surface microbuckles in the regions corresponding to the precipitation zones (PZs). This effect has not been observed and quantified for macroscopic, wet-gel systems in which precise measurement of the topography of the soft surface is problematic. Because our experiments were performed on relatively hard (even when wetted), dry gels, it was possible to determine the surface topography using profilometry (Figure 2c). We found that the height, h_n, of the nth ring increases linearly with x_n (Figure 2d, left) but its width, $w_n = w$, does not change with n. This trend reflects the fact that all $Ag_2Cr_2O_7$ produced is collected in the precipitation zones[27] (Figure 2d, right). To see

this, we note that the nth ring is formed from silver dichromate precipitated between radial locations z_{n-1} and z_n, whose relative positions $(x_n - z_{n-1})/(z_{n-1} - x_{n-1})$ are constant.[18,28] Consequently, the amount of $Ag_2Cr_2O_7$ collected by each ring (per unit length of the ring) is roughly proportional to x_n. Assuming that the degree of surface deformation is proportional to the amount of silver dichromate at a given location[29] and approximating the shape of the buckled precipitation zone by a triangle of base w and height h_n, we expect h_n to be proportional to x_n, as observed experimentally. We briefly mention that the profilometric method of determining the width of the precipitation zones is much more precise than an often used optical method. In fact, according to a microscopic inspection, w_n increases linearly with n; this result is an artifact caused by minute quantities of deeply colored $Ag_2Cr_2O_7$ present in the tails of the precipitation zones.

Our experimental method allowed not only the creation of PP patterns from arbitrary geometries of stamped features (Figure 3a and b) but also the control of them at the level of stochastic phenomena. It has been long known that PP can develop into (chiral) spirals or can lead to the formation of discontinuities (defects) propagating in the direction perpendicular to the precipitation zones; none of these effects, however, could be experimentally controlled. We were able to induce spirals whose chiralities were determined by the chirality of a pattern in the stamp; that is, the chiralities of the spirals were the same as those of the stamped patterns (Figures 3c and 4d). In patterns with sharp contours of the features, we achieved controlled propagation of defects whose morphologies could be subdivided into three types: (i) fork dislocations propagated in wedges (Figures 3d and 4e), (ii) loop-in-band defects originating from the tips of stamped "spikes" (Figure 3f), and (iii) band multiplications observed at the sharp turns in channel geometries (Figure 3e). All of these effects were reproducible and were quantified in 3D numerical simulations.

The ability to rephrase the observed dependencies of $1 + p$ on D, d, and H in the form of the MP law suggests strongly that microscopic PP is best described by the so-called nucleation-and-growth model (NG).[15−18,30] This model assumes that $Ag_2Cr_2O_7$ formed prior to the creation of rings is free to diffuse throughout the gel. If the local concentration of free silver dichromate (denoted henceforth C) reaches some threshold value C^*, then nucleation occurs followed by aggregation into immobile precipitate D. With these assumptions and denoting the concentration of silver cations as A and the concentration of potassium dichromate as B, the NG model can be written in the form of partial differential reaction−diffusion (RD) equations because both the planar geometry of the stamped feature and the depth of the gelatin layer affect PP in our system. These equations are 3D (i.e., all concentrations depend on $\mathbf{r} = (x, y, z)$). In dimensionless variables $\tau = tD_A/(D + d)^2$ and $\mathbf{x} = \mathbf{r}/(D + d)$, they read

$$\frac{\partial A}{\partial \tau} = \nabla^2 A - 2R(A, B)\,\theta(A^2B - K)$$

$$\frac{\partial B}{\partial \tau} = \frac{D_B}{D_A}\nabla^2 B - R(A, B)\,\theta(A^2B - K)$$

$$\frac{\partial C}{\partial \tau} = \frac{D_C}{D_A}\nabla^2 C + R(A, B)\,\theta(A^2B - K) - C\theta(C - C^*) - CN(C, D)$$

$$\frac{\partial D}{\partial \tau} = C\theta(C - C^*) + CN(C, D)$$

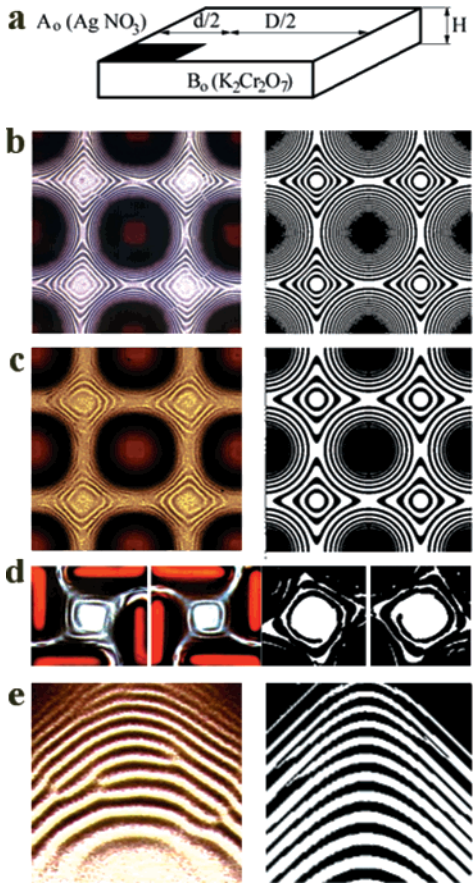

Figure 4. (a) Schematic representation of a unit cell used in numerical simulations. The black area represents the feature−gel interface. (b) PP patterns obtained in the experiment (left) and in numerical simulations (right) for an array of $d = 150$ μm squares separated by $D = 750$ μm for a gel thickness of $H = 36$ μm. (c) Same geometry as in b but for $H = 126$ μm. (d) Experimental (pictures in the left column) and modeled (pictures in the right column) spirals obtained from chiral stamps; the chiralities of the spirals are the same as those of the patterns used to create them. (e) Fork dislocation in a wedge. The left picture is an optical micrograph, and the right one is a simulated pattern.

where K is the solubility product and $D_{A,B,C}$ are the diffusion coefficients of A, B, and C, respectively. The step functions θ were used because reaction, nucleation, and aggregation are much faster than the transport of components. The term $R(A, B)$ reflects the stochastcity of the reaction and is given by[17] $R(A, B) = \delta[c_r + (1 - c_r)r]\,\exp(-s^2)$, with r being a random number from the interval [0, 1], $s = (2A - B)/(2A + B)$, and δ calculated from equation $(A - \delta)^2(B - \delta/2) = K$; the coefficient $0 < c_r < 1$ determined the degree of stochasticity of the reaction ($c_r = 1$ corresponds to the deterministic nucleation, when $c_r = 0$ the process is totally probabilistic). The term $N(C, D)$ determined whether aggregation occurred at a given location. It was defined as follows: (i) if some aggregate was already present at a given location $\mathbf{r}$, $D(\mathbf{r}) > 0$, then $N(C, D) = 1$, or if $D(\mathbf{r}) = 0$ but there was some precipitate in the vicinity d$\mathbf{r}$ of location $\mathbf{r}$ and if the concentration of C was above the aggregation threshold $C(x) > D^*$, then $N(C, D) = 1$; otherwise, $N(C, D) = 0$. The four RD equations were solved using appropriate boundary conditions and experimental concentrations and with parameters $D_{C,D}$, C^*, D^*, and c_r optimized for a qualitative fit with three different experimental patterns.[31] These optimized parameters were used in all subsequent calculations.

The results of simulations were in excellent agreement with experiment (Figure 4). The model not only accounted for the observed dependencies of $(1 + p)$ on $d/(d+D)$ and H in simple

geometries (Figures 1d and 2b, respectively) but also captured subtle geometrical differences between patterns on thick and thin gels (Figure 4b and c). It also reproduced effects that are highly stochastic in nature: the creation of chiral patterns originating from chiral stamps (Figure 4d) and the propagation of defects in discontinuous geometries (Figure 4e). In this respect, the reliability of our simulations allowed us to use them to guide the experiment. For example, the ranges of angles in wedge and spike geometries for which the defects would propagate (less than $130 \pm 10°$ for wedges and greater than $230 \pm 10°$ for spikes) were first estimated in simulations and subsequently verified in experiments.

4. Conclusions

In summary, we have developed an experimental system that allows for the scaling of periodic precipitation phenomena to microscopic dimensions and to study these phenomena with unprecedented accuracy in arbitrary geometries. Our work demonstrates, for the first time, that the morphologies and periodicities of PP patterns can be controlled precisely by the geometry of the system and that even highly stochastic processes (e.g., induction of chiral patterns or propagation of defects) can be brought under experimental control. On the fundamental level, our findings allow for the rephrasing of heuristic laws based on the concentrations of the participating chemicals in terms of the dimensions of the system. The scaling arguments we developed are supplemented by unique, fully 3D simulations of PP, and because these simulations faithfully reproduce all of the features of the patterns observed in the experiment, they can be a valuable tool in the *rational* design of PP systems of desired morphologies. The combination of theory and experiment we described is ripe for use in microtechnology (e.g., in the fabrication of quasi-3D optical elements (Figure 3b) or microstructured materials). Our experimental method can be further extended to study systems in which the stamps and/or gels would contain more than one periodically precipitating chemical (Figure 3g and h). We expect that in such systems the coupling between different PP reactions (either through common reagents or through the intermodulation of diffusion coefficients) would be reflected in unusual morphologies of PP patterns and might lead to emergent/complex phenomena.[32−34]

Acknowledgment. This work was supported by Northwestern University start-up funds. B.A.G. gratefully acknowledges financial support from the Camille and Henry Dreyfus New Faculty Awards Program. M.F. was supported by a NATO Scientific Fellowship.

References and Notes

(1) Liesegang, R. E. *Naturwiss. Wochenschr.* **1986**, *11*, 353.
(2) Chernavskii, D. S.; Polezhaev, A. A.; Muller, S. C. *Physica* D **1991**, *54*, 160.
(3) Sultan, R. F. *Phys. Chem. Chem. Phys.* **2002**, *4*, 1253.
(4) Chopard, B.; Droz, M.; Magnin, J.; Racz, Z.; Zrinyi, M. *J. Phys. Chem. A* **1999**, *103*, 1432.
(5) Heinsch, H. K. In *Crystals in Gels and Liesegang Rings*; Cambridge University Press: Cambridge, England, 1988; Chapter 5.
(6) Avnir, D.; Kagan, M. *Nature* **1984**, *307*, 717.
(7) Hunt, P. A.; Mitchell, P. B.; Paton, T. R. *Geoderma* **1977**, *19*, 105.
(8) Ball, P. *The Self-Made Tapestry: Pattern Formation in Nature*. Oxford University Press: Oxford, England, 2001.
(9) LeVan, M. E.; Ross, J. *J. Phys. Chem.* **1987**, *91*, 6300.
(10) Krug, H.-J.; Brandtstadter, H. *J. Phys. Chem. A* **1999**, *103*, 7811.
(11) Racz, Z. *Physica A* **1999**, *274*, 50.
(12) Muller, S. C.; Ross, J. *J. Phys. Chem. A* **2003**, *107*, 7997.
(13) Jablczynski, C. K. *Bull. Soc. Chim. Fr.* **1923**, *33*, 1592.
(14) Matalon, R.; Packter, A. *J. Colloid. Sci.* **1955**, *10*, 46.
(15) Chopard, B.; Luthi, P.; Droz, M. *Phys. Rev. Lett.* **1994**, *72*, 1384.
(16) George, J.; Paul, I.; Varughese, P. A.; Varughese, G. *Pramana* **2003**, *60*, 12591.
(17) Heinsch, H. K. In *Periodic Precipitation*; Pergamon Press: Oxford, England, 1991.
(18) Antal, T.; Droz, M.; Magnin, J.; Racz, Z.; Zrinyi, M. *J. Chem. Phys.* **1998**, *109*, 9479.
(19) Even small droplets of dimensions similar to those of the features in the stamps that we used ($100-300\ \mu$m) gave transient precipitation zones that extended $\sim 0.8-1$ mm from their edges; the first, thick rings appeared at $x_0 > 1$ mm.
(20) Fialkowski, M.; Campbell, C. J.; Bensemann, I. T.; Grzybowski, B. A. *Langmuir* **2004**, *20*, 3513.
(21) Irrespective of their size, droplets of $AgNO_3$ solution placed on dry gelatin did not produce PP patterns. Immediately after application, a thick layer of precipitate formed along the perimeter of each drop; this layer prevented the transport of silver cations into the gel (and also the spreading of the droplet).
(22) (i) Stamps were prepared from an 8% w/w solution of high-strength-gel agarose (OmniPur, EM Science, Darmstadt, Germany) in deionized water. This solution was heated in a microwave chamber for 90 s to dissolve the agarose and then degassed for 40 s to remove air bubbles. Next, an 8-mm-thick layer of the hot solution was poured onto the surface of an oxidized PDMS (poly(dimethylsilioxane)) master having the negative of the desired bas-relief pattern embossed on its surface. After gelation at room temperature, the layer was cut into 1 cm × 1 cm stamps. (ii) Thin gelatin films were prepared from a 10% w/w solution of gelatin (gelatin B, Bloom, Sigma-Aldrich) in deionized water. This solution was stirred and heated to 75 °C for 30 min before potassium dichromate (0.5% w/w) was added. The mixture was heated for another 3 min, poured onto the surface of an oxidized Petri dish (VWR), and dried under vacuum for 24 h.
(23) The transport of water into the bulk was a diffusive process against the osmotic pressure because of the salt present in the gel. Diffusion coefficient D_w was estimated by measuring the water uptake of a series of dry gelatin films doped with $K_2Cr_2O_7$ and of varying thicknesses, placed in conformal contact with unpatterned blocks of agarose; the amounts of adsorbed water were related to D_w through a theoretical model described in detail in ref 20.
(24) The amount, ΔB, of B consumed in the precipitation zone is roughly proportional to $B_0 d$. Because the characteristic diffusion times are much longer than the time of creation of this zone, the initial concentration of B in the interval $(D + d)$ between the features decreases by $\Delta B \approx B_0 d/(D + d)$ before PP starts.
(25) We[20] and others[35] suggested that this layer has a different molecular structure than the bulk of the gel; anomalous wetting and absorptivity properties of this layer reflect this difference.
(26) Because the rate of transfer of Ag^+ is driven by the concentration gradient at the agarose/gelatin interface and because all Ag^+ cations below the stamped feature are constantly being depleted, the flux of silver ions entering the gel does not change appreciably as long as the reaction front propagates.
(27) In addition, all $K_2Cr_2O_7$ from between the rings was used to form them. This was verified experimentally by staining the developed patterns with a solution of silver nitrate: upon staining, the inter-ring regions remained uncolored, indicating that there was no $K_2Cr_2O_7$ left therein.
(28) Droz, M.; Magnin, J.; Zrinyi, M. *J. Chem. Phys.* **1999**, *110*, 9618.
(29) Matsuo, E. S.; Tanaka, M. *Nature* **1992**, *358*, 482.
(30) The alternative, post-nucleation model is not able to account for the observed scaling laws.
(31) The RD equations were solved using the Crank-Nicholson scheme on a three-dimensional square grid $N_x \times N_y \times N_z$, with $N_x = N_y$ and N_z varying from 100 to 200 and from 20 to 80, respectively. For all species, von Neumann boundary conditions were used. Additionally, for $A(x, \tau)$ Dirichlet boundary conditions, $A(x, \tau) = A_0$, were applied. The initial conditions were $A(x, \tau = 0) = C(x, \tau = 0) = D(x, \tau = 0) = 0$ and $B(x, \tau = 0) = B_0$. The input parameters were $A_0 = 1.0$ M, $B_0 = 0.1$ M, and $K = 10^{-11}$;[36] the ratio of the diffusion coefficients was $D_A/D_B/D_C = 1{:}0.06{:}0.04$; and the nucleation and aggregation thresholds were ($C^* = 0.08$, $D^* = 0.06$) and $c_r = 0.9$.
(32) Nicolis, G.; Prigogine, I. *Self-Organization in Nonequlibrium Systems: From Dissipative Structures to Order Through Fluctuations.* Wiley: New York, 1977.
(33) Grzybowski, B. A.; Wiles, J. A.; Whitesides, G. M. *Phys. Rev. Lett.* **2003**, *90*, 083903.
(34) Grzybowski, B. A.; Whitesides, G. M. *Science* **2002**, *296*, 718.
(35) Harmon, M. E.; Kuckling, D.; Frank, C. W. *Macromolecules* **2003**, *36*, 162.
(36) Zhuk, N. P. *Zh. Fiz. Khim.* **1954**, *28*, 1690.